Progress In Electromagnetics Research C, Vol. 173, 83–91, 2026

PIER C

(Received 2 July 2026, Accepted 10 August 2026, Scheduled 31 August 2026)

Fast Monostatic Scattering Analysis of Large-Scale Periodic Arrays Using an MMV-CS-CM-SED Method

Yukun Ding[1], Zhonggen Wang[1], Wenyan Nie[2,*], and Quan Sun[3]

[1]*School of Electrical and Information Engineering, Anhui University of Science and Technology, Huainan 232001, China*
[2]*School of Mechanical and Electrical Engineering, Huainan Normal University, Huainan 232001, China*
[3]*School of Automation, Nanjing Institute of Technology, Nanjing 211167, China*

ABSTRACT: Conventional methods face prohibitive computational overhead for multi-aspect monostatic scattering analysis of large-scale finite periodic arrays (LFPAs) due to repetitive preprocessing and full-matrix inversion under wide-angle multiple-incidence scenarios. To address this challenge, this paper proposes an efficient multi-measurement vector compressive sensing framework combined with characteristic mode subdomain extraction (MMV-CS-CM-SED). It extracts excitation-independent CM-SED basis functions from a 3×3 coupled subarray, forming a reusable sparse dictionary. Furthermore, we introduce a uniform spatial sampling strategy based on golden-section low-discrepancy sequences, which drastically reduces matrix filling by extracting only a small portion of impedance matrix rows. Finally, the method leverages the joint sparsity of multi-angle coefficients through an MMV model to accelerate the solution process. Numerical results demonstrate that, compared to the accurate subdomain entire-domain (ASED) and method of moments (MoM), the proposed method achieves high radar cross-section (RCS) accuracy while reducing total matrix filling and computational time by over 70%, validating its efficiency and accuracy for large-scale array electromagnetic analyses.

1. INTRODUCTION

Large-Scale Finite Periodic Arrays (LFPAs) advance stealth technology, wireless communications, and related fields with their unique electromagnetic characteristics [1, 2]. In electromagnetic scattering characterization of radar targets, analysis of monostatic RCS is particularly critical, yet requires continuous plane-wave sweeping over the full angular spatial domain. Conventional full-wave approaches, such as the MoM [3, 4], lead to severe memory usage and time bottlenecks for massive unknowns and multiple right-hand-side excitations. To mitigate this limitation, a variety of macro basis function (MBF) techniques have been developed, including the synthetic function method (SFM) [5, 6], characteristic basis function method (CBFM) [7, 8], and accurate subdomain entire-domain (ASED) basis functions [9–11]. However, for monostatic multi-angle sweeping tasks, external excitations vary drastically, forcing conventional MBF methods to regenerate new basis sets repeatedly for distinct angular intervals, thus prolonging preprocessing time. Moreover, full assembly and reduced matrix inversion remain mandatory and prevent breaking computational constraints for large-scale arrays. In recent years, periodic characteristic mode analysis (PCMA) built on characteristic mode theory has offered a novel pathway to tackle this challenge [12–14]. Since extracting characteristic modes (CMs) solely depends on the intrinsic physical topology and material properties, they are excitation-independent and can be losslessly reused for arbitrary incidences.

Meanwhile, compressive sensing (CS) techniques have been introduced into electromagnetic computation [15–17]. Nevertheless, existing PCMA methods generally neglect the strong inter-element coupling [18], and conventional CS models suffer from oscillatory artifacts due to ill-constructed sensing matrices. To account for the strong mutual coupling and edge effects in large-scale arrays, the subdomain-entire-domain (SED) basis function method is incorporated by constructing a 3×3 coupled subarray [19, 20], which provides a physically robust sparse dictionary for accurately modeling local electromagnetic interactions., Additionally, to handle multi-angle incidences in monostatic scenarios, the MMV model exploits the joint sparsity of modal coefficients across scanning angles [21, 22].

To address the above drawbacks, this paper proposes an MMV-CS-CM-SED approach for fast monostatic analysis of LFPAs. The major contributions of this work are summarized as follows. First, virtual cells construct a 3×3 coupled subarray for CM extraction, yielding a globally coupled yet excitation-independent CM-SED basis dictionary. Second, different from purely random subsampling schemes in conventional CS, this paper proposes a uniform spatial sampling strategy based on golden-section low-discrepancy sequences. This strategy enables efficient extraction of global physical information at an extremely low sampling ratio and eliminates numerical oscillations. Third, the massive full-array sweeping problem is transformed into a highly flat MMV overdetermined equation by exploiting the joint sparsity of monostatic sweeping coefficients. Numerical results demonstrate that the proposed method achieves high electromagnetic accuracy while break-

* Corresponding author: Wenyan Nie (wynie5240@163.com).

ing memory and runtime bottlenecks inherent to conventional algorithms.

2. THEORY

In this section, we systematically introduce the theoretical foundation of the proposed MMV-CS-CM-SED method. We begin with the conventional MoM formulation and compressive sensing principles, then demonstrate the construction of the excitation-independent CM-SED sparse dictionary, and finally establish the MMV reconstruction model.

2.1. MoM Formulation

Assume that the LFPAs to be analyzed consist of N periodic unit cells as illustrated in Fig. 1(a), where each unit cell contains M_0 unknowns. When electromagnetic modeling is performed via the MoM, the electromagnetic scattering problem over the surface of the full array can be converted into the following equation based on the electric field integral equation (EFIE).

$$\mathbf{ZJ} = \mathbf{V} \tag{1}$$

where $\mathbf{Z}$ denotes the $NM_0 \times NM_0$ full-array impedance matrix; $\mathbf{J}$ is the unknown coefficient vector of surface-induced currents to be solved; and $\mathbf{V}$ represents the incident-field excitation vector. Conventional MoM solves this matrix equation directly, involving a total of NM_0 unknowns, which becomes computationally infeasible for large N. To compress the unknown variables, we introduce CS theory on the MoM matrix equation.

2.2. Method of the CS Theory

CS theory recovers sparse signals from low-dimensional observations via a measurement matrix uncorrelated with the sparse basis. In electromagnetic scattering problems, the induced current $\mathbf{J}$ is generally non-sparse under Rao-Wilton-Glisson RWG basis functions. Nevertheless, when SED basis functions or CBFM are adopted as the sparse transform basis $\mathbf{J}^{CM\text{-}SED}$, the expansion coefficients α of induced currents exhibit favorable sparsity:

$$\mathbf{J} = \mathbf{J}^{CM\text{-}SED}\alpha \tag{2}$$

where $\mathbf{J}^{CM\text{-}SED}$ is the global sparse ictionary matrix. Conventional CS-MoM [23] and CS-CBFM [24] extract partial rows from the full-array impedance matrix $\mathbf{Z}$ and excitation vector $\mathbf{V}$ using random or fixed-step sampling. Substituting these terms into Eq. (1) yields a compressed measurement equation with respect to the sparse coefficient α:

$$\Phi\mathbf{Z}\mathbf{J}^{CM\text{-}SED}\alpha = \Phi\mathbf{V} \tag{3}$$

which can be expressed as follows:

$$\Theta\alpha = \widetilde{\mathbf{V}} \tag{4}$$

where $\Theta = \widetilde{\mathbf{Z}}\mathbf{J}^{CM\text{-}SED}$ is the sensing matrix, and $\widetilde{\mathbf{V}}$ is the reduced-dimensional excitation vector.

In conventional CS, due to high sparse basis dimension and low sampling ratios, Eq. (4) is severely underdetermined, requiring sophisticated algorithms like orthogonal matching pursuit (OMP) or sparse Bayesian learning (SBL) [25]. Nevertheless, the CM-SED basis functions proposed in this paper drastically reduce the dimensionality of unknowns from a physical perspective. Combined with the MMV multi-angle measurement model, within the electromagnetic computation framework constructed herein, the row dimension of the measurement matrix Φ is strictly larger than the column dimension of the sparse coefficient vector α. Thus, Eq. (4) forms a highly overdetermined linear system, eliminating the need for iterative reconstruction. Instead, QR decomposition-based least squares can be used for direct solving, circumventing numerical oscillations while cutting computational overhead.

2.3. Extraction of the CM and Coupling SED

To construct a physically meaningful sparse basis independent of external excitations, this work introduces CM theory. The impedance matrix of a reference unit cell is obtained via the MoM, and CMs are extracted by formulating the generalized eigenvalue equation as follows:

$$\mathbf{X}^{ref}\mathbf{J}_i^{ref} = \lambda_i \mathbf{R}^{ref}\mathbf{J}_i^{ref} \tag{5}$$

where $\mathbf{X}^{ref}$ and $\mathbf{R}^{ref}$ denote the imaginary and real parts of the reference unit-cell impedance matrix, and $\mathbf{J}_i^{ref}$ stands for the ith characteristic current corresponding to the eigenvalue λ_i. According to CM theory, smaller eigenvalues imply greater mode contribution to scattering. Modal Significance (MS) is introduced for mode selection:

$$MS = \frac{1}{|1 + j\lambda_i|} \tag{6}$$

In practical applications, modes with $MS > 0.7$ are considered significant [26]. For reciprocal lossless media, characteristic currents are strictly orthogonal, ensuring the linear independence of the sparse dictionary.

Considering the edge effects of finite arrays and strong mutual coupling between elements, extracting CMs merely from a single reference unit cell will drastically degrade numerical accuracy. Therefore, drawing on the idea of SED basis functions, this paper constructs a 3×3 coupled subarray by introducing virtual cells as illustrated in Fig. 1(b) for CM extraction, which yields nine types of CM-SED basis functions, incorporating globally dominant coupling effects. According to their physical structure within the subarray, these nine categories are classified as: the left-upper corner cell (LUCC), upper edge cell (UEC), right-upper corner cell (RUCC), left edge cell (LeEC), inner center cell (IC), right edge cell (REC), left-lower corner cell (LLCC), lower edge cell (LoEC), and right-lower corner cell (RLCC). Subsequently, in accordance with the spatial position matching criterion, these nine CM-SED basis functions with distinct local coupling characteristics are precisely mapped to each unit cell of the full array. Based on these partially mutually independent local basis functions, a strictly diagonalized global sparse dictionary matrix for the full array can be constructed:

$$\mathbf{J}^{CM\text{-}SED} = \mathrm{diag}(\mathbf{J}_1^{CM\text{-}SED}, \mathbf{J}_2^{CM\text{-}SED}, \ldots, \mathbf{J}_N^{CM\text{-}SED}) \tag{7}$$

Combined with Eq. (2), the surface-induced current $\mathbf{I}_{\text{full}}$ over the full array can be projected into the characteristic mode do-

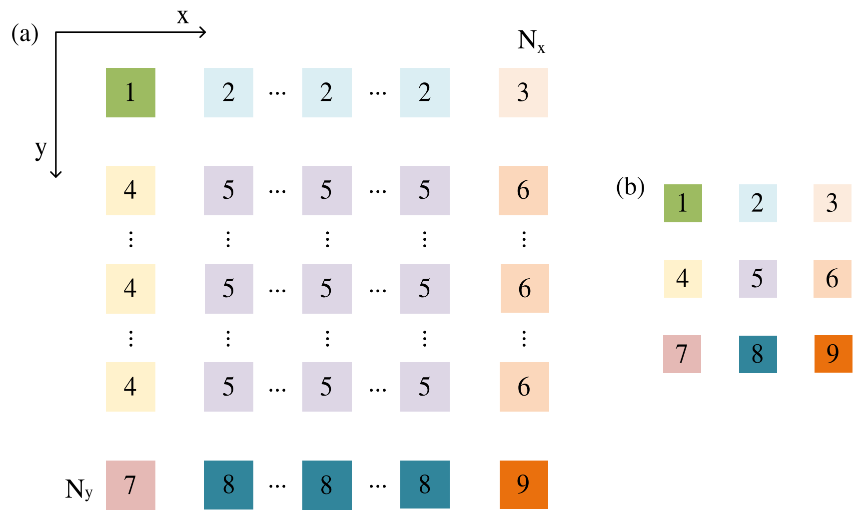

FIGURE 1. $N_x \times N_y$ finite periodic arrays and 3×3 subarrays.

main as a sparse linear expansion:

$$\mathbf{I}_{\text{full}} = \mathbf{J}^{CM\text{-}SED}\alpha \tag{8}$$

where α is the global sparse coefficient vector composed of modal system matrices for each unit.

2.4. Proposed Method

In monostatic electromagnetic scattering calculations, a radar is required to scan the target over the full angular spatial domain. Assume that the monostatic radar scans a total of L distinct incident angles over the azimuth or elevation plane, and the incident field corresponding to each angle forms an excitation vector that continuously varies with the observation angle. In the Single Measurement Vector (SMV) CS model described, the CS equation in Eq. (4) must be solved independently for each of these L angles. This not only introduces massive computational time that multiplies with the number of sweeping angles, but is also highly susceptible to local noise interference at certain specific angles, leading to single-angle reconstruction failure.

To overcome the above drawbacks, this work fully exploits the excitation independence of CMs and incorporates an MMV joint sparsity model into the monostatic scattering computation framework. During monostatic angular sweeping, although the amplitude and phase gradient of the external excitation field vary drastically, the expansion coefficient vectors α of CM-SED basis functions at different incident angles share an identical non-zero support set within the CM domain, following the mode expansion principle of CM theory. It is essential to further validate the physical foundation of this overdetermined MMV model. The required sparsity of the coefficient matrix is inherently established by the CM mode truncation described in Section 2.3. Since the modes satisfying $MS > 0.7$ are retained, the number of unknowns is drastically compressed. Meanwhile, because CMs are intrinsic eigenfunctions independent of external excitations, the support consistency across different illumination angles is naturally guaranteed. Consequently, the non-zero support set of the coefficient matrix A remains strictly identical for all L scanning angles, confirming physical validity of the MMV joint sparsity model. Based on this physical property, we column-concatenate the subsampled equations corresponding to all L incident angles to construct the following MMV compressive reconstruction model:

$$\Theta\mathbf{A} = \widetilde{\mathbf{E}} \tag{9}$$

where $\mathbf{A} = [\alpha_1, \alpha_2, \dots, \alpha_L]$ denotes the global multi-angle modal coefficient matrix of dimension $mN \times L$; N denotes the total number of unit cells; and m is the number of high-efficiency CMs extracted for each unit cell.

$$\widetilde{\mathbf{E}} = \left[\widetilde{\mathbf{V}}_1, \widetilde{\mathbf{V}}_2, \dots, \widetilde{\mathbf{V}}_L\right] \tag{10}$$

where $\widetilde{\mathbf{E}}$ stands for the joint subsampled excitation matrix of dimension $M \times L$. It can be observed that the proposed method extracts the core CMs with the highest radiation efficiency inside the array from a physical perspective, drastically compressing the column dimension of the global dictionary matrix to satisfy $m \ll M_0$, where M_0 is the number of RWG unknowns per unit cell. Low-discrepancy sequences effectively eliminate clustering effects inherent in pure random sampling. It evenly distributes the selected observation edge heights throughout the array structure, ensuring comprehensive coverage of arbitrary polarized edges. This feature fundamentally avoids matrix pathology caused by spatial aliasing. Accordingly, even at an extremely low physical spatial sampling ratio, the row dimension M of the measurement matrix strictly satisfies $M \gg mN$. This property inherently makes Eq. (10) a highly overdetermined matrix equation. To numerically verify the overdetermined claim, we examine the matrix dimensions in our numerical implementation. For the 10×10 array, each unit cell has $M_0 = 240$ unknowns. After CM extraction, we retain $m = 6$ dominant modes per cell, yielding a global sparse coefficient matrix of column dimension $N_m = 100 \times 6 = 600$. Meanwhile, due to the golden-section sampling strategy, the measurement matrix extracts only $M = 3840$ rows (16% sampling). Clearly, the row dimension $M = 3840$ strictly satisfies $M \gg N_m = 600$. This dimensional inequality confirms that Eq. (10) is a highly overdetermined system, requiring no

TABLE 1. Comparison of computational time for different methods.

Model	Methods	Filling Impedance(s)	Solving Time(s)	Total Time(s)
Square array	ASED	1323.49	1.59	1325.08
	Proposed method	362.62	4.72	367.34
Square ring array	ASED	8761.95	26.79	8788.74
	Proposed method	2190.49	56.36	2246.85

iterative sparse reconstruction algorithms like OMP or SBL. In most conventional electromagnetic applications of compressive sensing, standard CS equations generally form underdetermined systems, which have to be solved via computationally expensive iterative algorithms, such as OMP and sparse Bayesian learning. In contrast, the proposed method not only endows the sensing matrix with a favorable condition number, but also allows Eq. (10) to eliminate spurious numerical oscillations originating from underdetermined reconstruction. For such an overdetermined system, the QR decomposition-based least squares method is adopted for direct non-iterative solving. Mathematically, this approach bypasses the bottlenecks of large-scale matrix inversion and sparse matching iterations existing in conventional schemes; meanwhile, matrix operations enable parallel processing of excitations corresponding to all L incident angles in a single run, substantially boosting the solving efficiency for full-angle sweeping. After solving Eq. (10) to acquire the global multi-angle modal coefficient matrix $\mathbf{A}$, multiply the CM-SED global sparse dictionary $\mathbf{J}^{CM\text{-}SED}$ constructed in Section 2.3 by the coefficient matrix $\mathbf{A}$ to rapidly recover the true surface induced current matrix $\mathbf{I}_{\text{full}}$ of the full array under all L incident angles:

$$\mathbf{I}_{\text{full}} = \mathbf{J}^{CM\text{-}SED}\mathbf{A} \tag{11}$$

Finally, the restored induced current can be used to accurately calculate the RCS of each individual station in the array.

3. COMPLEXITY ANALYSIS

In this section, a theoretical complexity comparison among the conventional MoM, the ASED method, and the proposed method is conducted from two key perspectives: impedance matrix filling and equation solving. This analysis highlights the computational efficiency bottlenecks overcome by our approach.

3.1. Impedance Matrix Filling and Measurement Matrix Construction Stage

Both MoM and ASED must fully pre-populate the original full-array impedance matrix Z under the Galerkin testing scheme, with double-integral evaluation complexity reaching $O((NM_0)^2)$. For large-scale arrays, memory and filling time scale quadratically with problem size, forming a primary bottleneck. The proposed method uses a physics-driven subsampling strategy, computing only the M_{row} rows corresponding to the measurement matrix Φ. This constructs a subsampled impedance matrix of dimension $M_{row} \times NM_0$, reducing complexity to $O(M_{row}NM_0)$. The extremely low physical sampling ratio drastically cuts matrix filling. Numerical results show that for the 10×10 square array, filling time drops from 1323.49 s (ASED) to 362.62 s (a 72.6% reduction). For the larger square ring array (78,600 unknowns), filling time decreases from 8761.95 s to 2190.49 s, saving over 6500 seconds.

3.2. Stage of Basis Function Generation and Solving

Both ASED and the proposed method operate on a 3×3 coupled subarray for basis generation, with single-solution complexity $O((9M_0)^3)$. The key distinction is reusability. ASED must regenerate basis functions for different angle intervals, multiplying generation time by the number of angles. In contrast, CMs are geometry-dependent intrinsic eigenfunctions; they are extracted once and reused for all incident angles, providing massive savings in wide-angle monostatic scans.

For equation solving, ASED requires inversion of a fully filled dimension-reduced impedance matrix with complexity $O(N^3)$, followed by back-substitution for each angle. Our sensing matrix Θ construction exploits the block-diagonal property of $J^{CM\text{-}SED}$, with complexity $O(M_{row}mN)$. During solving, physical dimension reduction ensures $m \ll M_0$ and sampling ensures $M_{row}\times \gg mN$. Thus, the MMV equation is highly overdetermined, allowing QR-decomposition least squares solving with complexity $O(M_{row}(mN)^2)$, processing all L angles simultaneously.

Notably, from Table 1, our method's solving time (4.72 s) is slightly higher than ASED (1.59 s) because ASED solves a reduced square matrix, whereas our QR decomposition handles an overdetermined system with row dimension $M_{row} = 3840$. However, this minor solving time increase is negligible compared to massive savings in matrix filling. For the square array, we sacrifice 3.13 s in solving to save 960.87 s in filling. For the square ring array, we trade 29.57 additional solving seconds for 6571.46 filling seconds. Since matrix filling is the dominant bottleneck for large periodic arrays, our method achieves total time reductions of 72.3% and 74.4% for the two arrays. As problem size expands from 24,000 to 78,600 unknowns, the saving remains stable and slightly improves. This aligns perfectly with the complexity analysis, in which our matrix filling scales linearly with unknowns, whereas conventional methods scale quadratically. Consequently, the computational advantage of our framework becomes increasingly pronounced as the array dimension grows.

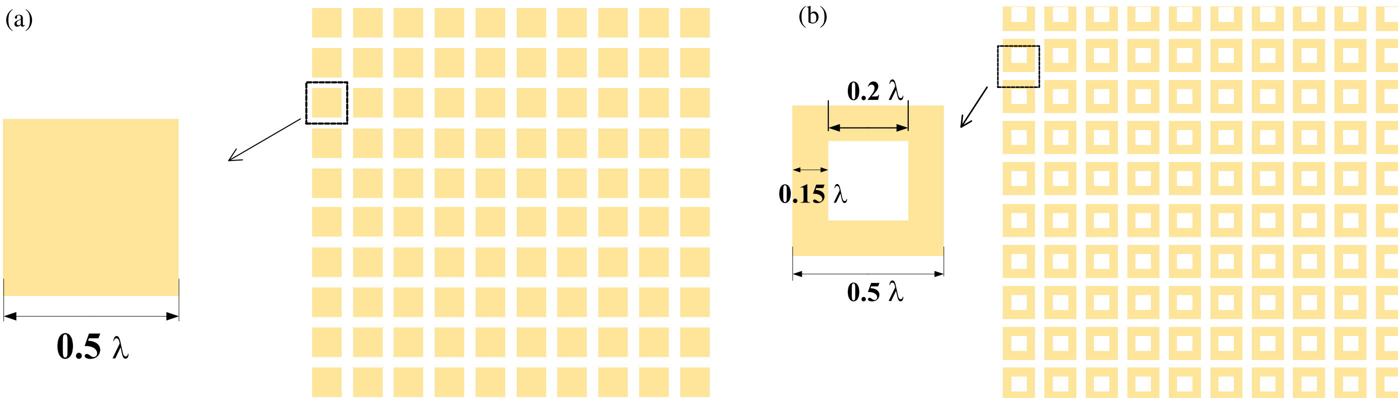

FIGURE 2. Geometric configurations of array structures: PEC square array and PEC square ring array.

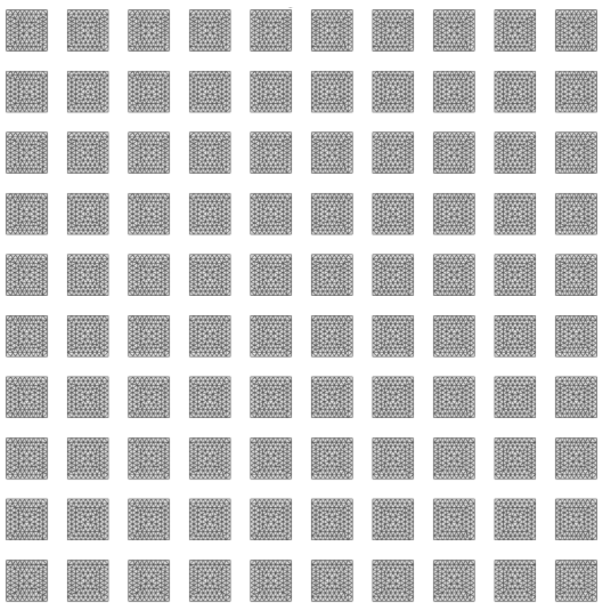

FIGURE 3. 10×10 Macroscopic structure and microscopic triangular mesh segmentation of PEC arrays.

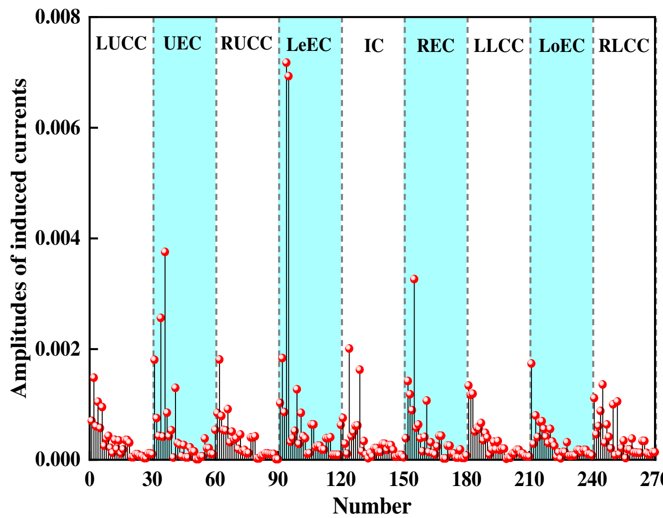

FIGURE 4. Amplitude of induced current coefficients on CM-SED basis functions.

4. NUMERICAL EXAMPLES AND RESULTS

In this section, to verify the efficiency and accuracy of the proposed MMV-CS-CM-SED method when analyzing electromagnetic scattering problems of LFPAs, numerical simulations are carried out for periodic arrays with different unit-cell geometric shapes. To objectively evaluate the proposed algorithm, the MoM's direct solving results are taken as the accuracy benchmark for all numerical results, and the traditional ASED basis function method is introduced as the efficiency comparison counterpart. The algorithm's accuracy is quantitatively evaluated via the root mean square error (RMSE), whose calculation formula is expressed as:

$$RMSE = \sqrt{\frac{1}{N_\theta}\sum_{i=1}^{N_\theta}\left|\sigma_{pro}(\theta_i) - \sigma_{MoM}(\theta_i)\right|^2} \tag{12}$$

where N_θ denotes the total number of angular sampling points for monostatic scanning; $\sigma_{MoM}(\theta_i)$ and $\sigma_{pro}(\theta_i)$ represent RCS values calculated by the conventional MoM and the proposed algorithm in this paper at the incident angle, respectively. This metric can intuitively reflect the overall fitting accuracy of the proposed method against the benchmark solution across the entire scanning angular range.

4.1. PEC Square Array

This section considers a 10×10 discrete perfect electric conductor (PEC) solid square array consisting of 100 physical elements. This array's geometry is shown in Fig. 2(a), and its macroscopic topology and detailed triangular mesh discretization are presented in Fig. 3. The central frequency is set to 1 GHz, and the side length of each array element is 0.5λ, where λ denotes the wavelength. Each square patch element is discretized via RWG basis functions, yielding a total of 24,000 unknowns. The monostatic incident wave adopts HH polarization, and the full-angle scanning range is $\theta \in [0°, 360°]$ $(\phi = 0°)$. Although the nine types of CM basis functions extracted from the 3×3 coupled subarray primarily characterize local coupling, their combination automatically adapts to the

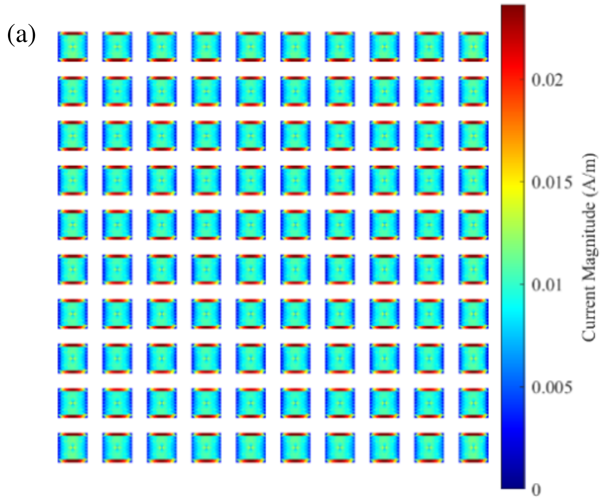

FIGURE 5. Square patch array surface current distribution MoM and the proposed method.

physical state of the full array through weighted coefficients when constructing the full-array dictionary matrix $\mathbf{J}^{CM\text{-}SED}$ due to the unique edge current features exhibited by boundary unit cells, specifically LUCC and UEC. As illustrated in Fig. 4, the amplitude of induced current coefficients in edge regions, including LUCC and LeEC, is significantly greater than that in central regions, demonstrating that this mapping approach accurately captures edge effects, and the resulting fidelity is sufficient to meet engineering accuracy requirements.

Figure 5 compares the surface current distributions obtained by MoM and the proposed method. As observed from the monostatic RCS curves plotted in Fig. 6, the results of the proposed MMV-CS-CM-SED method overlap nearly perfectly with the reference solutions from direct MoM solving. Even at broadside angles or certain specific non-resonant angular regions, the proposed method accurately captures deep nulls and broad peaks of the RCS response. This verifies that the constructed CM-SED sparse basis and MMV joint reconstruction model can effectively preserve the array's global electromagnetic coupling information.

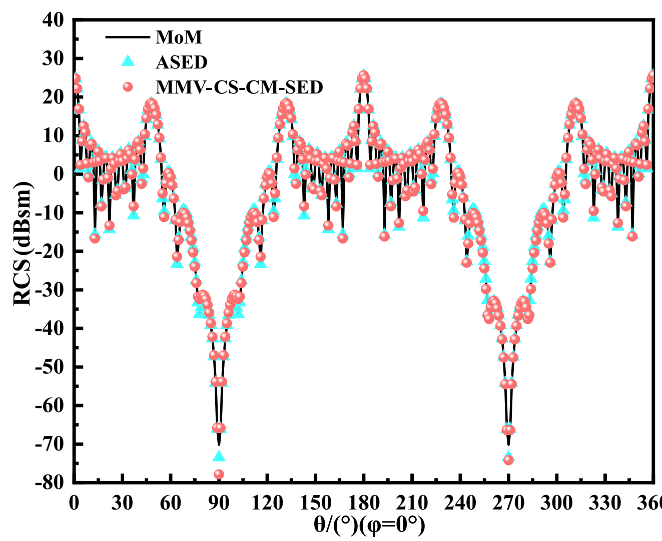

FIGURE 6. Monostatic RCS of the 10×10 PEC square array.

Table 1 details the comparison of time consumption at different computational stages between the proposed method and the conventional ASED macro basis function method. The numerical data lead to the following conclusions: In the impedance matrix filling stage, the conventional ASED method requires full computation of the full-array-sized impedance matrix, resulting in a fixed filling time of 1323.48 seconds. In contrast, the proposed method adopts a physics-driven low-discrepancy sequence subsampling strategy; only a tiny fraction of rows required by the measurement matrix are filled, drastically cutting the filling time to 362.61 seconds, corresponding to a reduction of approximately 72.6%. The solving time column combines both basis function generation and equation solving process to align with the computational workflow. For the conventional ASED method, the total solving time is 1.59 seconds. This includes solving a 3×3 subarray via the standard MoM for basis generation and direct inversion of the dimension-reduced matrix to solve the final equation. For the proposed method, the solving time is 4.72 seconds, which encompasses the extraction of characteristic modes by solving a generalized eigenvalue equation on a 3×3 coupled subarray, alongside the subsequent direct non-iterative solving of the highly underdetermined MMV equation using QR decomposition. Although the proposed method's solving time is marginally higher than that of the ASED method, it remains well within an acceptable range. Ultimately, the total computational time for the proposed method is 367.34 seconds, compared to 1325.08 seconds for the ASED method. This demonstrates that the proposed MMV-CS-CM-SED approach successfully reduces the overall computation time by approximately 72.3% while maintaining high accuracy, primarily due to the immense savings achieved during the impedance filling phase. This prominent advantage mainly stems from the drastic reduction in impedance matrix filling time. Moreover, as the array scale further expands, the advantage of the proposed method in avoiding full-matrix filling will become even more pronounced.

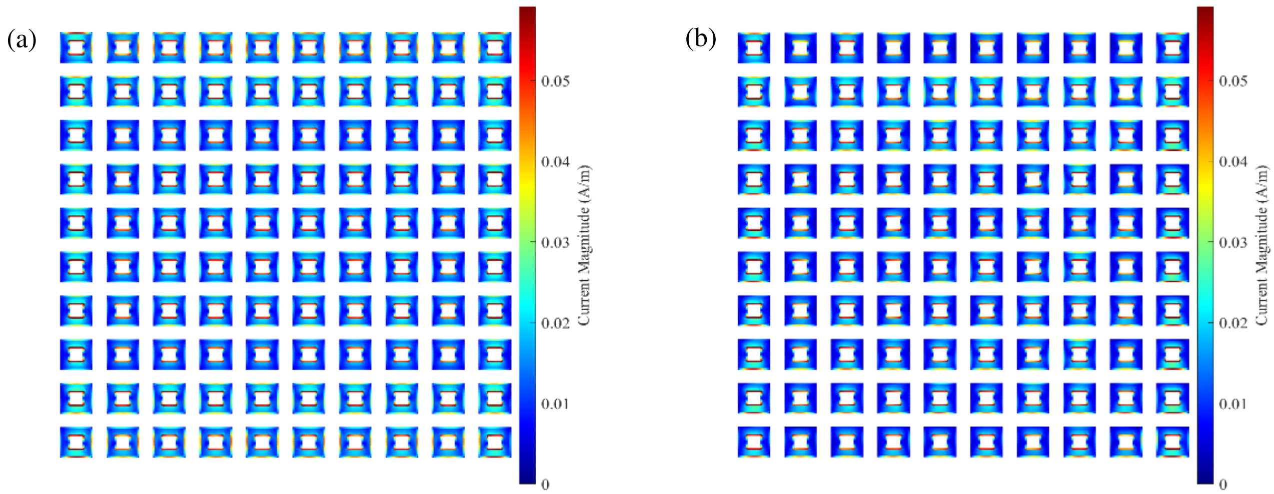

FIGURE 7. Square ring patch array surface current distribution MoM and the proposed method.

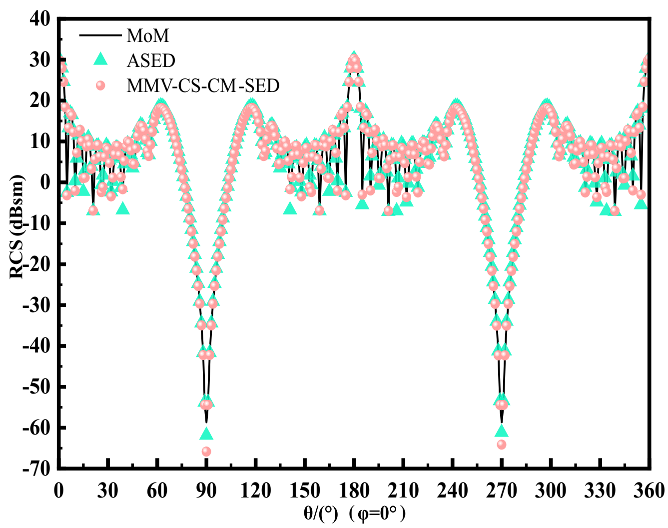

FIGURE 8. Monostatic RCS of the 10×10 PEC square ring array.

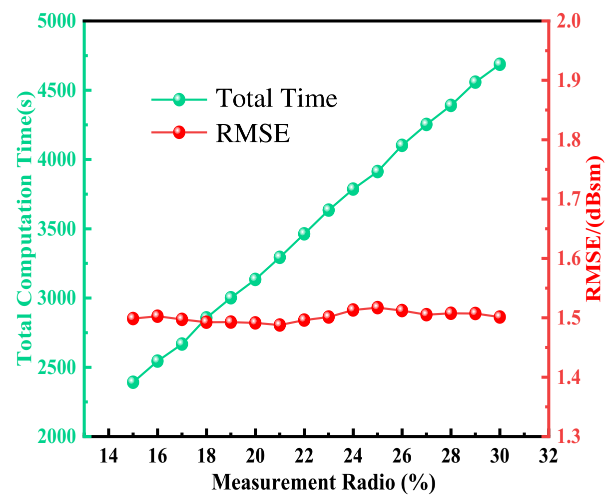

FIGURE 9. Total computational time and RMSE under different sampling ratios.

4.2. PEC Square Ring Array

This section considers a discrete PEC square ring array consisting of 100 physical elements. This array's geometry is illustrated in Fig. 2(b). The central frequency is set to 1 GHz. The outer side length of the ring element is 0.5λ, while its inner side length is 0.2λ. Each square ring element is discretized via RWG basis functions, yielding a total of 78,600 unknowns. The monostatic incident wave adopts Horizontal-Horizontal (HH) polarization, and the full-angle scanning range is $\theta \in [0°, 360°]$ $(\phi = 0°)$. Fig. 7 compares the surface current distributions obtained by MoM and the proposed method.

As observed from monostatic RCS curves in Fig. 8, results of the proposed MMV-CS-CM-SED method overlap nearly perfectly with reference solutions from direct MoM solving, even at broadside angles or complex resonant nulls. This verifies that the constructed CM-SED sparse basis and MMV joint reconstruction model can effectively preserve the array's global electromagnetic coupling information. Calculation results show that the RMSE of this array across the full scanning angular range remains consistently below 1.6 dBsm, satisfying the requirements of high-precision electromagnetic computation. For the square ring array, the conventional ASED method required 8761.95 seconds for full impedance matrix filling. Benefiting from the physics-driven subsampling strategy, the proposed method drastically cut this to 2190.48 seconds, a 75.0% reduction. Regarding the combined solving time, the ASED method spent 26.78 seconds, whereas the proposed method required 56.36 seconds. Consequently, the total computation time is 2246.85 seconds for the proposed method versus 8788.73 seconds for ASED, achieving an overall reduction of 74.4%. Compared to the solid square array, the computational advantages become increasingly pronounced as the problem size expands, further verifying the scalability of the proposed method in avoiding full matrix filling.

The RMSE stabilizes at approximately 1.6 dBsm and is primarily determined by two contributing factors. The first is mode truncation errors arising from the $MS > 0.7$ criterion during 3×3 subarray CM extraction, and the second is reconstruction residuals caused by the physical sampling of rows and columns from the impedance matrix. Fig. 9 reveals that after the

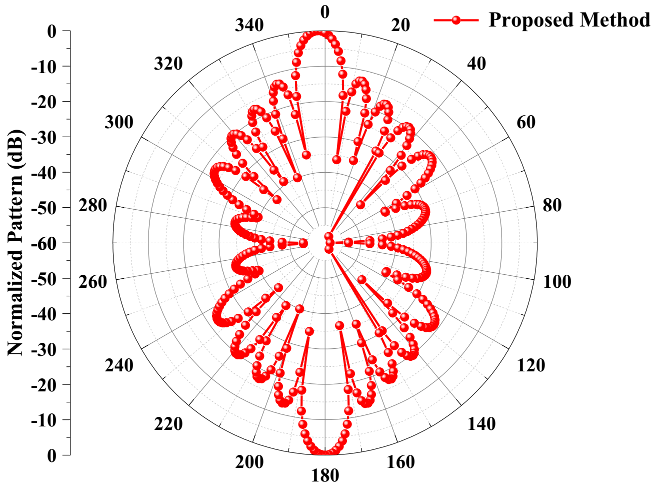

FIGURE 10. Normalized equivalent receiving pattern of the 10×10 PEC square ring array.

sampling ratio exceeds 16%, the RMSE becomes insensitive to further increases in the sampling ratio. This indicates that the error of the proposed method is predominantly constrained by physical boundary approximations caused by CM mode truncation, rather than the condition number of the sampling matrix.

To demonstrate the robustness of the proposed method, we compare its performance with conventional compressive sensing approaches reported in the literature [16, 18]. Unlike traditional CS-based methods, which rely on random sampling and often suffer from ill-conditioned sensing matrices, the proposed golden-section low-discrepancy sampling strategy ensures a well-conditioned measurement matrix. Furthermore, while the SBL method in [25] requires sophisticated iterative reconstruction and can be sensitive to noise, our method transforms the problem into a highly overdetermined linear system, allowing a direct non-iterative solution, such as QR decomposition. As shown in Fig. 9, the proposed method achieves stable RMSE values even when the sampling ratio is reduced to 16%. This stability across different sampling ratios, along with the avoidance of iterative recovery, strongly validates the robustness of the proposed method against modeling errors and numerical oscillations.

4.3. Equivalent Radiation Pattern Verification

This section provides an equivalent radiation pattern of the finite periodic array based on physical properties of scattering. It must be clarified that the primary scope of this paper is passive monostatic scattering, and the analyzed array structures do not contain active feed networks. Consequently, the absolute active antenna gain cannot be defined or numerically derived within the current analytical framework.

However, according to the Reciprocity Theorem in electromagnetics, the receiving pattern of a passive lossless array is strictly identical to its transmitting radiation pattern. Since the plane-wave incidence in monostatic scattering corresponds to the array operating in the receiving mode, the accurately solved induced currents I_{full} from the proposed method can be directly used to compute the equivalent far-field pattern via standard far-field integration.

For demonstration, the 10×10 PEC square ring array is taken as a representative example. By applying the far-field integration to the extracted currents, the normalized equivalent bistatic scattering pattern is obtained. As shown in Fig. 10, this pattern physically represents the array's spatial filtering characteristics. It is found to contain distinct major lobes and sidelobes that align well with the theoretical directivity of the periodic array. While the absolute gain values remain unavailable due to the passive scattering nature, this equivalent pattern verification successfully provides valuable engineering intuition regarding the array's radiation characteristics.

5. CONCLUSION

This paper proposes an MMV-CS-CM-SED method for the fast monostatic analysis of large-scale finite periodic arrays, representing the first integration of MMV, CS, CM, and SED for this application. The method extracts excitation-independent CM-SED bases via coupled subarrays to avoid repeated preprocessing. Using a golden-section low-discrepancy physical sampling strategy, it eliminates full impedance matrix filling and transforms the conventional ill-posed, underdetermined reconstruction into a stable, highly overdetermined equation. Numerical results confirm high robustness and accuracy while achieving significantly reduced computational time compared to MoM and ASED, demonstrating a highly efficient and effective strategy for large-scale array electromagnetic analyses.

ACKNOWLEDGEMENT

This work was supported in part by the Natural Science Research Project of Anhui Educational Committee under Grant No. 2025AHGXZK31006, in part by the Research Foundation of Jiangsu Engineering Research Center for Bionics Control Technology and Equipment under No. FSKZ202503, in parts by the Anhui International Joint Research Center for Ancient Architecture Intelligence and Multi-Dimensional Modeling under No. GJZZX2025KF03.

REFERENCES

[1] Ou, M., Y. Sun, F. Huang, and P. Wang, "Enhancing ASED basis function method with compressive sensing for fast analysis of large-scale finite periodic arrays," *Microwave and Optical Technology Letters*, Vol. 67, No. 3, e70168, 2025.

[2] Xiao, K., F. Zhao, S.-L. Chai, J.-J. Mao, and J. L.-W. Li, "Scattering analysis of periodic arrays using combined CBF/P-FFT method," *Progress In Electromagnetics Research*, Vol. 115, 131–146, 2011.

[3] Harrington, R. F., *Field Computation by Moment Methods*, Macmillan, New York, 1968.

[4] Rao, S., D. Wilton, and A. Glisson, "Electromagnetic scattering by surfaces of arbitrary shape," *IEEE Transactions on Antennas and Propagation*, Vol. 30, No. 3, 409–418, 1982.

[5] Matekovits, L., V. A. Laza, and G. Vecchi, "Analysis of large complex structures with the synthetic-functions approach," *IEEE Transactions on Antennas and Propagation*, Vol. 55, No. 9, 2509–2521, 2007.

[6] Matekovits, L., G. Vecchi, G. Dassano, and M. Orefice, "Synthetic function analysis of large printed structures: The solution space sampling approach," in *IEEE Antennas and Propagation Society International Symposium. 2001 Digest. Held in Conjunction with: USNC/URSI National Radio Science Meeting (Cat. No.01CH37229)*, Vol. 2, 568–571, Boston, MA, USA, 2001.

[7] Wang, Z.-G., W.-Y. Nie, and H. Lin, "Characteristic basis functions enhanced compressive sensing for solving the bistatic scattering problems of three-dimensional targets," *Microwave and Optical Technology Letters*, Vol. 62, No. 10, 3132–3138, 2020.

[8] Konno, K., Q. Chen, and R. J. Burkholder, "Numerical analysis of large-scale finite periodic arrays using a macro block-characteristic basis function method," *IEEE Transactions on Antennas and Propagation*, Vol. 65, No. 10, 5348–5355, 2017.

[9] Lu, W. B., T. J. Cui, Z. G. Qian, X. X. Yin, and W. Hong, "Accurate analysis of large-scale periodic structures using an efficient sub-entire-domain basis function method," *IEEE Transactions on Antennas and Propagation*, Vol. 52, No. 11, 3078–3085, 2004.

[10] Du, P., P. D. Xu, and S. Zhang, "An efficient wideband analysis method based on ASED basis function method and improved fir for large-scale finite periodic structures," in *2019 International Symposium on Antennas and Propagation (ISAP)*, 1–3, Xi'an, China, 2019.

[11] Du, P., G. Zheng, C. Wang, and W. J. Fu, "Efficient wideband computation of electromagnetic scattering by finite periodic structures combining ASED basis function with frequency-independent reaction," *IEEE Antennas and Wireless Propagation Letters*, Vol. 17, No. 2, 234–237, 2018.

[12] Cheng, G. S. and C.-F. Wang, "A novel periodic characteristic mode analysis method for large-scale finite arrays," *IEEE Transactions on Antennas and Propagation*, Vol. 67, No. 12, 7637–7642, 2019.

[13] Wang, Z., P. Wang, Y. Sun, and W. Nie, "Fast analysis of bistatic scattering problems for three-dimensional objects using compressive sensing and characteristic modes," *IEEE Antennas and Wireless Propagation Letters*, Vol. 21, No. 9, 1817–1821, 2022.

[14] Guo, F., Z. Wang, Y. Sun, W. Nie, P. Wang, and J. Wu, "Novel characteristic mode basis functions accelerating iteration convergence of CMM for analyzing electromagnetic scattering problems," *Applied Computational Electromagnetics Society Journal (ACES)*, Vol. 38, No. 8, 594–601, 2023.

[15] Candes, E. J. and M. B. Wakin, "An introduction to compressive sampling," *IEEE Signal Processing Magazine*, Vol. 25, No. 2, 21–30, 2008.

[16] Wang, Z., B.-Z. Wang, and W. Shao, "Efficient construction and solution of MoM matrix equation with compressed sensing technique," *Journal of Electromagnetic Waves and Applications*, Vol. 29, No. 5, 683–692, 2015.

[17] Xiang, J., Z. Wang, H. Yuan, and W. Nie, "Energy-based adaptive Krylov subspace basis functions method for solving bistatic scattering problems," *Progress In Electromagnetics Research C*, Vol. 158, 151–159, 2025.

[18] Wang, Z., F. Guo, W. Nie, Y. Sun, and P. Wang, "Principal component analysis accelerated the iterative convergence of the characteristic mode basis function method for analyzing electromagnetic scattering problems," *Progress In Electromagnetics Research M*, Vol. 117, 129–138, 2023.

[19] Xiang, W., W. Yang, and W. Lu, "Fast subentire-domain basis functions method for analysis of composite finite periodic structures with dielectric-conductor cells," *IEEE Antennas and Wireless Propagation Letters*, Vol. 22, No. 2, 233–237, 2023.

[20] Guo, F., T. Liu, B. Song, W. Yang, and W. Lu, "Efficient analysis of electromagnetic scattering in large-scale finite periodic structures using characteristic modes," *IEEE Antennas and Wireless Propagation Letters*, Vol. 24, No. 12, 4970–4974, 2025.

[21] Cotter, S. F., B. D. Rao, K. Engan, and K. Kreutz-Delgado, "Sparse solutions to linear inverse problems with multiple measurement vectors," *IEEE Transactions on Signal Processing*, Vol. 53, No. 7, 2477–2488, 2005.

[22] Ou, M., Y. Sun, Z. Wang, and P. Wang, "Multiple-measurement-vectors compressive sensing enhanced CBFM for analyzing wide-angle scattering problems of three-dimensional objects," *IEEE Antennas and Wireless Propagation Letters*, Vol. 24, No. 7, 1635–1639, 2025.

[23] Qi, Q., Y. Fan, X. Cao, Y. Liu, M. Kong, Z. Huang, and X. Wu, "An improved compressive sensing-based model for efficient analysis of monostatic electromagnetic scattering problems," *IEEE Microwave and Wireless Technology Letters*, Vol. 35, No. 4, 388–391, 2025.

[24] Ou, M., Y. Sun, and C. Shi, "Compressive sensing enhanced multilevel characteristic basis function method for analyzing electrically large scattering problems," *IEEE Antennas and Wireless Propagation Letters*, Vol. 23, No. 2, 593–597, 2024.

[25] Zhang, H. H., W. E. I. Sha, and L. J. Jiang, "Fast monostatic scattering analysis based on Bayesian compressive sensing," in *2017 International Applied Computational Electromagnetics Society Symposium — Italy (ACES)*, 1–2, Firenze, Italy, 2017.

[26] Chen, Y. and C.-F. Wang, "Characteristic mode theory for dielectric resonators," *Characteristic Modes: Theory and Applications in Antenna Engineering*, 143–185, Wiley 2015.